Hydroxyl Radical at the Air−Water Interface

ARTICLE *in* JOURNAL OF THE AMERICAN CHEMICAL SOCIETY · JANUARY 2005

Impact Factor: 12.11 · DOI: 10.1021/ja045552m · Source: PubMed

5 AUTHORS, INCLUDING:

Martina Roeselova
Academy of Sciences of the Czech Republic
46 PUBLICATIONS **893** CITATIONS
SEE PROFILE

Bruce C Garrett
Pacific Northwest National Laboratory
296 PUBLICATIONS **11,954** CITATIONS
SEE PROFILE

Supporting Information

Hydroxyl radical at the air-water interface.

Martina Roeselová, John Vieceli, Liem X. Dang, Bruce C. Garrett, and Douglas J. Tobias*

Department of Chemistry, University of California, Irvine, California 92697, and Environmental Molecular Sciences Laboratory, Pacific Northwest National Laboratory, Richland, Washington 99352.

Computational details

Potential parameters and validation of the force field. Both OH and water were modeled using empirical potentials that explicitly include induced polarization. The water molecules were described using the three-site water model of Caldwell and Kollman (POL3).[1] The Lennard-Jones parameters of the OH oxygen and hydrogen were also taken from POL3 water. The remaining potential parameters were adopted from our previous work:[2] The permanent dipole of OH radical was modeled by partial charges of −0.4 *e* on oxygen and 0.4 *e* on hydrogen, with the O–H bond length of 0.967 Å. The molecular polarizability of OH, 1.07 Å^3, which was obtained as the mean value of the diagonal elements of the polarizability tensor calculated at the MP2/aug-cc-pvtz level, was assigned to the oxygen atom.

The present OH parametrization represents a refinement of the force field used in our previous study,[2] which underestimated the OH–water binding as well as the OH hydration free energy. Adopting the Lennard-Jones parameters for the OH oxygen and hydrogen from the POL3 water model improved substantially the performance of the force field in terms of the OH hydration, yielding the free energy of solvation $\Delta G_s = -3.0 \pm 0.1$ kcal/mol (experimental value $\Delta G_{s,exp} = -3.9 \pm 0.3$ kcal/mol[3,4]). The OH–water binding is somewhat overestimated by the new potential, the stabilization energy of the OH…H_2O complex being -7.4 kcal/mol (the ab initio values reported in the literature span the interval between 5.5 and 6.7 kcal/mol[5-7]). However, the force field yields a correct geometry of the OH…H_2O complex, with the OH acting as a proton donor. The structural properties of larger clusters involving more than one water molecule are also in agreement with the ab initio results that predict the cluster structures, in which OH participates in two hydrogen bonds (acting both as a proton donor and proton acceptor) to be the energetically most favorable ones. In this connection, it is interesting to note that polarizability seems to be important for reproducing correctly the structures of the OH-water clusters with the empirical force field. In simulations with a non-polarizable potential, the OH radical was found to act predominantly as proton donor, forming only one hydrogen bond to the nearest water molecule.[8]

Sampling simulation. NVT molecular dynamics simulation was carried out on five OH radicals solvated in water. A water slab with two vacuum/liquid interfaces was employed, using 864 water molecules in a 30(x) × 30(y) × 100(z) Å simulation box. The *z*-axis is perpendicular to the water surface. Periodic boundary conditions were applied in all three dimensions. The thickness of the water slab was about 33 Å. The initial conditions were constructed from the final configuration of the water slab equilibrated for 500 ps at $T = 300$ K by exchanging five water molecules inside the bulk liquid for OH radicals and placing the five water molecules into the gas phase region above the slab. A 20 ps equilibration run with an integration time step of 0.1 fs was performed, at the end of which all five OH radicals were still fully solvated inside the bulk water, close to the middle of the slab. The equilibration was then followed by a 3 ns sampling run with a time step of 1 fs. The temperature of the system was maintained at 300 K using the Berendsen scheme with a coupling constant of 0.5.[9] All bond lengths were constrained to their equilibrium values using SHAKE.[10] An interaction cutoff of 12 Å was employed. A smooth particle mesh Ewald method was used to account for the long-range Coulomb interactions.[11] The positions of OH radicals were stored every picosecond. All MD simulations were performed using the AMBER program package.[12]

During the simulation, the OH radicals diffused through the interior of the water slab, they were, however, predominantly located in either of the two interfacial regions. Desorption of OH from the surface was also observed a number of times, resulting in the OH radical leaving the simulation box and, due to the periodic boundary conditions, its replica entering the simulation box with the same velocity from the opposite side. The 3 ns simulation yielded a fairly symmetric OH density profile (see Figure 1 in the communication). The intervals on the *z*-axis in Figure 1b, in which the water signal decreases from the bulk density value to zero, correlate with the two interfacial regions of the water slab. The OH density profile was scaled by an arbitrarily chosen number such that its maximum approximately matches the water bulk density value.

Scattering simulations. The adsorption kinetics of OH radical was studied using the same water slab system as described above. Configurations of the liquid to be used for the accommodation study were generated from a 250 ps NVE run following a 500 ps NVT equilibration at T = 300 K. Storing the positions and velocities every 50 ps yielded five different configurations of the water slab. 250 initial conditions for the scattering simulations were then prepared by placing a single OH radical about 15 Å above the interface at different grid points in the *xy* plane at z = 30 Å, and assigning the velocities of each of the two atoms from a Maxwell-Boltzmann distribution at 300 K, subject to the constraint that the z-component of the center of mass velocity is directed towards the surface. The trajectories were run for a total of 90 ps. During the first 15 ps, the position and velocity of the incoming OH radical were stored every 0.1 ps for a detailed kinetic energy analysis that was correlated with the position. During the final 75 ps, the position was stored every 1.0 ps.

Thermal accommodation and mass accommodation coefficients. From the above 250 initial conditions, in 3 cases the OH radical was deflected away from the liquid slab due to a very small initial value of the z-component of velocity. Thus, the total number of molecules impinging on the surface equals 247 (n_{imp} = 247). 12 trajectories resulted in scattering of OH from the surface (n_{scat} = 12), and 235 in accommodation of OH at the interface (n_{acc} = 235). For 12 out of the 235 trajectories, for which OH was initially accommodated at the interface, the hydroxyl radical later desorbed back into the gas phase (n_{des} = 12). For 142 trajectories OH remained adsorbed on the surface until the end of the 90 ps simulation (n_{ads} = 142), located on average rather deep in the interface at a z-position that correlates with the Gibbs dividing surface. For 81 trajectories OH diffused inside the water slab and became fully absorbed in the bulk liquid (n_{abs} = 81). The above numbers of adsorbed and absorbed OH radicals were determined at the end of the 90 ps trajectories based on the z-position of the oxygen atom of the OH radical. The OH was considered adsorbed when having the oxygen atom located between the 10% and 90% values of the liquid water density, and absorbed when being at a density greater than 90% of the liquid water density. The z-coordinate values corresponding to the 90% and 10% of the liquid water density for the 30 Å × 30 Å × 100 Å box with 864 molecules are 12.8 Å and 16.4 Å, respectively. From the kinetic energy analysis, it was found that, when approximately 5 Å above the liquid, the approaching OH radical is accelerated towards the surface as well as rotationally excited. In majority of cases (235 of 247), the collision of OH with the surface was followed by a fast dissipation of the excess kinetic energy within 4 ps of impact, resulting in thermal accommodation of OH at the interface. This yields for the thermal accommodation coefficient, S, defined as a ratio of the number of molecules equilibrated to the liquid temperature relative to the number of molecules impinging on the liquid surface ($S = n_{acc} / n_{imp}$), a value of S = 0.95. The mass accommodation coefficient, α, is defined as a ratio of the number of gas molecules incorporated into the liquid relative to the number of molecules impinging on the liquid surface. Trajectories for which OH radicals remain adsorbed for 90 ps can still contribute to the value of α. The probability, p, that an adsorbed OH radical will be incorporated into the bulk after 90 ps can be estimated from the available data for 90 ps as the number of trajectories for which OH became absorbed in the bulk liquid divided by the sum of those trajectories for which OH became absorbed and those for which OH first accommodated at the surface and then desorbed, $p = n_{abs} / (n_{abs} + n_{des}) = 0.87$. This yields for the mass accommodation coefficient $\alpha = (n_{abs} + p\, n_{ads}) / n_{imp} = 0.83$.

Free energy profile. A somewhat smaller system with 600 water molecules in a 26.3 × 26.3 × 76.3 Å simulation cell, yielding a water slab of a thickness of approximately 30 Å, was employed for calculating the free energy profile for transfer of an OH radical across the air/water interface. The free energy profile was calculated as a potential of mean force using a constrained molecular dynamics technique.[13] The radical is transferred along the normal to the interface (z). At each z-position of the solute, incremented by 1 Å, the averaging of the force exerted on the solute was done over 350 ps after an initial 100 ps equilibration period. The error of the calculated free energy values (± 0.1 kcal/mol) was estimated by averaging separately over the first 150 ps and the last 150 ps of the simulation at each z-position of the solute and taking the difference between the corresponding two values of free energy.

The free energy difference, $\Delta F(z_s)$, between a state when the solute is located at z_s and a reference state when the solute is at z_0 can be calculated as follows

$$\Delta F(z_s) = F(z_s) - F_0 = -\int_{z_0}^{z_s} \langle f_z(\zeta) \rangle d\zeta \ . \qquad (1)$$

In the above expression, $f_z(\zeta)$ is the z-component of the total force exerted on the solute at a given z-position, z_s, averaged over the canonical ensemble. Here, F_o is chosen as the free energy of the system with the hydroxyl radical located in the gas phase. Equation 1 is defined in a canonical (NVT) ensemble, and yields a Helmholtz free energy difference (ΔF). In our simulation, the total volume of the system is fixed. However, due to the fact that the open interfaces allow the volume of the liquid water to fluctuate, the conditions of the simulation actually resemble the isothermal-isobaric (NPT) ensemble. Thus, the free energies calculated from the simulation can be directly compared to the experimentally accessible Gibbs free energies (ΔG).[14]

Henry's law constant and the solvation free energy. From the free energy difference between two points z_1 and z_2 on the free energy profile, $\Delta G_{12} = \Delta G(z_2) - \Delta G(z_1)$, one can evaluate the corresponding concentration ratio of the solute species

$$c_2/c_1 = \exp(-\Delta G_{12} / RT). \quad (2)$$

In the above expression, R is the universal gas constant, and T is the temperature. By choosing z_1 in the gas phase and z_2 in the liquid, the calculated concentration ratio can be compared to the empirical Henry's law constant. The Henry's law constant k_H is usually defined as the molar concentration c_{aq} of a species in the aqueous phase divided by its partial pressure p_g in the gas phase

$$k_H = c_{aq} / p_g \quad (3)$$

Henry's law constant can, however, be also written as a dimensionless ratio of the molar concentrations or number densities in the aqueous and gas phases[15]

$$k_H^{cc} = c_{aq} / c_g \quad (4)$$

These two constants differ by a RT factor, and are related to the solvation free energy ΔG_s of the solute species at infinite dilution as follows

$$k_H^{cc} = k_H \cdot RT = \exp(-\Delta G_s / RT) \quad (5)$$

The standard solvation free energy ΔG_s^o corresponding to the standard state of $p_0 = 1$ atm gas pressure, temperature $T_0 = 298$ K, and aqueous concentration $c_0 = 1$ M differs from ΔG_s at infinite dilution by 1.9 kcal/mol according to the following equation[16]

$$\Delta G_s^o = \Delta G_s + RT \ln(RTc_0 / p_0) \quad (6)$$

The experimental value of the solvation free energy of OH in the 1 atm gas and 1 M aqueous standard state at $T = 298$ K is $\Delta G_s^o = -2 \pm 0.4$ kcal/mol,[17] and yields Henry's law constant $k_H = 30$ M/atm.[15,17,18] According to Eq. 6, the solvation free energy at infinite dilution is $\Delta G_{s,exp} = -3.9$ kcal/mol. This value corresponds to the transfer of a single OH radical across the air/water interface from the gas phase to the liquid phase, in accordance with the conditions under which the free energy profile is calculated in our simulation.

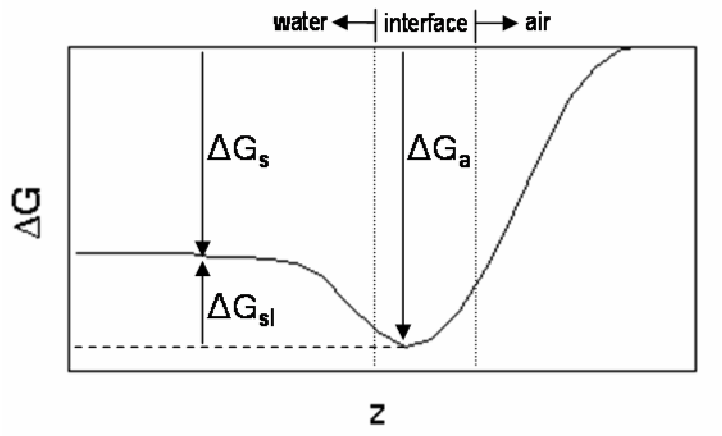

Figure 1S. Schematic diagram of a free energy profile for transferring a gas phase molecule accross the air/water interface. The interfacial region is indicated by the dotted lines. ΔGs denotes the free energy of solvation, ΔGa the free energy of adsorption on the water surface, and ΔGsl the free energy difference associated with moving the solute from the surface into the bulk.

To achieve an agreement with the experimental value of the OH free energy of solvation, $\Delta G_{s,exp}$, in a simulation employing empirical potentials represents a nontrivial task, as the asymptotic value of ΔG in the liquid phase depends strongly on the choice of the force field. However, the existence and depth of the surface minimum on the free energy profile seems to be rather robust, as very similar results were obtained for different OH and water force fields as well as using different methodology to calculate the free energy profile.[8,19]

Atmospheric implications.

The fact that the free energy profile for transfer of an OH radical across the air/water interface exhibits a minimum in the interfacial region indicates propensity of the hydroxyl radical for the interface. Under equilibrium conditions, the equilibrium between the OH in the gas phase and in the liquid (corresponding to the Henry's law and the solvation free energy ΔG_s in Figure 1S) can be split into two parts: the equilibrium between the OH in the gas phase and at the surface (corresponding to the adsorption free energy ΔG_a), and the equilibrium between the OH adsorbed on the surface and the OH dissolved in the liquid (free energy difference ΔG_{sl}). These free energy values are related through $\Delta G_s = \Delta G_a + \Delta G_{sl}$ (see Figure 1S). For the average daytime concentration of OH in the troposphere[20] $c_g = 5 \times 10^6$ radicals/cm^3 and $k_H = 30$ M/atm, the Henry's law yields the aqueous OH concentration $c_{aq} = 3.7 \times 10^9$ radicals/cm^3. Combining the experimental free energy of solvation $\Delta G_{s,exp} = -3.9$ kcal/mol and the calculated free energy difference $\Delta G_{sl} = 1.1$ kcal/mol between the surface and bulk state results in the free energy of adsorption $\Delta G_a = -5$ kcal/mol. This free energy difference, according to Eq. 2 for z_1 in the gas phase and z_2 at the interface, corresponds to the surface concentrations of OH $c_{surf} = 2.3 \times 10^{10}$ radicals/cm^3.

The surface activity of the OH radical opens some interesting possibilities for OH reactions with the oxidizable species, both inorganic and organic, at the air/water interface. For example, in a study of the reaction of gas phase OH radicals with deliquesced NaCl particles, it was shown that the experimental observations, which could not be explained based on the known gas and liquid phase chemistry, were consistent with a reaction of OH with chloride ions at the air/water interface.[21] There is a body of evidence showing that, in addition to inorganics, organic species are likely to be present at the aqueous atmospheric surfaces, e.g., of sea-salt aerosol and cloud droplets. Organic compounds can be removed from the ocean surface as the sea-water droplets are ejected into the air,[22,23] or they can be scavenged onto the surfaces of the aerosol particles and cloud droplets from the air.[24] Thus, the availability of OH radicals at enhanced concentration on the surface where also the oxidizable organic species are present may be important for understanding the mechanisms of atmospheric processing of the organic material. Recently, for instance, a heterogeneous reaction was proposed to rationalize the rapid oxidation of methanol to formaldehyde observed in field measurements of cloud droplets interacting with a plume from biomass burning.[25]

The impact of the surface enhancement of OH on atmospheric reactions will depend on a number of factors, including particle size, kinetics of its reaction with other species and possible enhancement of the second reactant in the interfacial region. Therefore, reactions of OH at the interface are likely to be more important for smaller particles where there is relatively more surface compared to the available bulk,[26] for less volatile, surface active reactants and for fast reactions where the OH reacts before it reaches the bulk.

The diffuso-reactive length, $l = \sqrt{\frac{D}{k'}}$, where D is the diffusion coefficient (typically ~10^{-5} cm^2 s^{-1} in liquids) and k' is the first order rate constant (s^{-1}) for the reaction of OH, is a measure of the distance from the interface in which the reaction occurs.[27] For a rapid reaction at the surface, one can consider $l = 1$ nm. Then $k' \sim 10^9$ s^{-1} = k[X], where k is the second order rate constant for the reaction between OH and some species X. The reactions of OH with most organics are very fast,[28] with k approaching 10^{10} M^{-1} s^{-1}. Thus, for a diffuso-reactive length of 1 nm, the concentration of X must be of the order of 0.1 M in the interface layer. This corresponds to a surface coverage of X of ~ 1% of a monolayer. While there are essentially no data on the surface composition of aqueous atmospheric particles, a coverage of this magnitude is reasonable under some conditions, e.g. in plumes from emission sources.

The calculations reported in this work show that OH radical is expected to be enhanced at the air/water interface. While our understanding of the role the surface OH can play in atmospheric processes is at its infancy, it is desirable that the possibility of the heterogeneous OH chemistry is taken into account when elucidating the mechanisms and kinetics of the atmospheric reactions.

References.

(1) Caldwell, J. W.; Kollman, P. A. *J. Phys. Chem.* **1995,** *99*, 6208-6219.
(2) Roeselová, M.; Jungwirth, P.; Tobias, D. J.; Gerber, R. B. *J. Phys. Chem. B* **2003,** *107*, 12690-12699.
(3) Hanson, D. R.; Burkholder, J. B.; Howard, C. J.; Ravishankara, A. R. *J. Phys. Chem.* **1992,** *96*, 4979-4985.
(4) Autrey, T.; Brown, A. K.; Camaioni, D. M.; Dupuis, M.; Foster, N. S.; Getty, A. *J. Am. Chem. Soc.* **2004,** *126*, 3680-3681.
(5) Cabral do Couto, P.; Guedes, R. C.; Costa Cabral, B. J.; Martinho Simoes, J. A. *J. Chem. Phys.* **2003,** *119*, 7344-7355.
(6) Hamad, S.; Lago, S.; Mejías, J. A. *J. Phys. Chem. A* **2002,** *106*, 9104-9113.

(7) Cooper, P. D.; Kjaergaard, H. G.; Langford, V. S.; McKinley, A. J.; Quickenden, T. I.; Schofield, D. P. *J. Am. Chem. Soc.* **2003,** *125*, 6048-6049.
(8) Roeselová, M.; Vieceli, J.; Dang, L. X.; Garrett, B. C.; Tobias, D. J., manuscript in preparation.
(9) Berendsen, H. J. C.; Postma, J. P. M.; van Gunsteren, W. F.; DiNola, A.; Haak, J. R. *J. Chem. Phys.* **1984,** *81*, 3684-3690.
(10) Ryckaert, J. P.; Ciccotti, G.; Berendsen, H. C. *J. Comput. Phys.* **1977,** *23*, 327-341.
(11) Essmann, U.; Perera, L.; Berkowitz, M. L.; Darden, T.; Lee, H.; Pedersen, L. G. *J. Chem. Phys.* **1995,** *103*, 8577-8593.
(12) Case, D. A.; Pearlman, D. A.; Caldwell, J.; Cheatham, T. E. I.; Ross, W. R.; Simmerling, C. L.; Darden, T. A.; Merz, K. M.; Stanton, R. V.; Cheng, A. L.; Vincent, J. J.; Crowley, M.; Tsui, V.; Radmer, R. J.; Duan, Y.; Pitera, J.; Massova, I.; Seibel, G. L.; Singh, U. C.; Weiner, P. K.; Kollman, P. A. *AMBER 6*, University of California, San Francisco: 1999. AMBER 6 was used for generating trajectories, modified version of AMBER 3 was used for free energy profile calculation.
(13) Ciccotti, G.; Ferrario, M.; Hynes, J. T.; Karpal, R. *Chem. Phys.* **1989,** *129*, 241-251.
(14) Taylor, R. S.; Garrett, B. C. *J. Phys. Chem. B* **1999,** *103*, 844-851.
(15) Sander, R. Compilation of Henry's law constants for inorganic nad organic species of potential importance in environmental chemistry. http://www/mpch-mainz.mpg.de/~sander/res/henry.html
(16) Ben-Naim, A.; Marcus, Y. *J. Chem. Phys.* **1984,** *81*, 2016-2027.
(17) Hanson, D. R.; Burkholder, J. B.; Howard, C. J.; Ravishankara, A. R. *J. Phys. Chem.* **1992,** *96*, 4979-4985.
(18) Takami, A.; Kato, S.; Shimono, A.; Koda, S. *Chem. Phys.* **1998,** *231*, 215-227.
(19) Vácha, R.; Slavíček, P.; Mucha, M.; Finlayson-Pitts, B. J.; Jungwirth, P. *J. Phys. Chem. B* **2004**, *submitted*.
(20) Mauldin, R. L.; Tanner, D. J.; Eisele, F. L. *J. Geophys. Res.-Atmos.* **1999,** *104*, 5817-5827.
(21) Knipping, E. M.; Lakin, M. J.; Foster, K. L.; Jungwirth, P.; Tobias, D. J.; Gerber, R. B.; Dabdub, D.; Finlayson-Pitts, B. J. *Science* **2000**, *288*, 301-306.
(22) Middlebrook, A. M.; Murphy, D. M.; Thomson, D. S. *J. Geophys. Res.* **1998**, *103*, 1664-1669.
(23) Ellison, G. B.; Tuck, A. F.; Vaida, V. *J. Geophys. Res.* **1999**, *104*, 11633-11641.
(24) Djikaev, Y. S.; Tabazadeh, A. *J. Geophys. Res. - Atmos.* **2003**, *108*, Art. No. 4689.
(25) Tabazadeh, A.; Yokelson, R. j.; Singh, H. B.; Hobbs, P. V.; Crawford, J. H.; Iraci, L. T. *Geophys, Res. Lett.* **2004**, *31*, Art. No. L06114.
(26) Mozurkewich, M. *Geophys. Res. Lett.* **1997**, *24*, 3209-3212.
(27) Finlayson-Pitts, B. J.; Pitts, J. N., Jr. *Chemistry of the Upper and Lower Atmosphere - Theory, Experiments, and Applications*; Academic Press: San Diego, 2000.
(28) National Institute of Standard, "NDRL/NIST Solution Kinetics Reference Database 40, Ver. 3.0," NIST, 1998.